



## Short communication

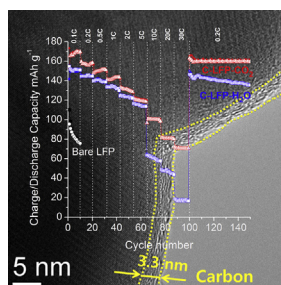
## Toward uniform and ultrathin carbon layer coating on lithium iron phosphate using liquid carbon dioxide for enhanced electrochemical performance

Seung-Ah Hong<sup>a</sup>, Dong Hyun Kim<sup>b</sup>, Kyung Yoon Chung<sup>b</sup>, Wonyoung Chang<sup>b</sup>, Jibeom Yoo<sup>c,d</sup>, Jaehoon Kim<sup>d,e,\*</sup><sup>a</sup> Department of Chemical and Biological Engineering, Korea University, 5-1 Anam Dong, Seongbuk-gu, Seoul 136-701, Republic of Korea<sup>b</sup> Center for Energy Convergence, Korea Institute of Science and Technology, Hwarangno 14-gil 5, Seongbuk-gu, Seoul 136-791, Republic of Korea<sup>c</sup> School of Advanced Materials Science and Engineering, Sungkyunkwan University, 2066, Seobu-Ro, Jangan-Gu, Suwon, Gyeonggi-Do 440-746, Republic of Korea<sup>d</sup> SKKU Advanced Institute of Nano Technology (SAINT), Sungkyunkwan University, 2066, Seobu-Ro, Jangan-Gu, Suwon, Gyeonggi-Do 440-746, Republic of Korea<sup>e</sup> School of Mechanical Engineering, Sungkyunkwan University, 2066, Seobu-Ro, Jangan-Gu, Suwon, Gyeonggi-Do 440-746, Republic of Korea

## HIGHLIGHTS

- Developing a carbon coating method using liquid carbon dioxide as a solvent.
- Ultrathin and uniform carbon layer coating on LiFePO<sub>4</sub> particles.
- Enhanced rate performance of LiFePO<sub>4</sub> using small amount of carbon.

## GRAPHICAL ABSTRACT



## ARTICLE INFO

## Article history:

Received 6 March 2014

Received in revised form

24 March 2014

Accepted 26 March 2014

Available online 3 April 2014

## Keywords:

Liquid carbon dioxide

Carbon coating

Lithium iron phosphate

Lithium secondary battery

## ABSTRACT

In this communication, uniform and ultrathin carbon coating on LiFePO<sub>4</sub> (LFP) particles are performed using liquid carbon dioxide (*l*-CO<sub>2</sub>)-based free-meniscus coating. The uniform and conformal coverage of the carbon layer on LFP with a thickness of 3.3 nm, and a uniform distribution of carbon on the entire surface of the LFP particle are confirmed. The carbon-coated LFP (C-LFP) with a carbon content of 1.9 wt.% obtained using *l*-CO<sub>2</sub>-based coating exhibits a discharge capacity of 169 mAh g<sup>-1</sup> at 0.1 C and 71 mAh g<sup>-1</sup> at 30 C, while much lower discharge capacity of 146 mAh g<sup>-1</sup> at 0.1 C and 17 mAh g<sup>-1</sup> at 30 C is observed when C-LFP with an optimized carbon content of 6.0 wt.% is prepared using conventional aqueous-based coating.

Crown Copyright © 2014 Published by Elsevier B.V. All rights reserved.

## 1. Introduction

In recent years, the development of lithium ion batteries for large-scale applications such as electric vehicles (EV) and energy storage systems (ESSs) has received considerable attention in both

\* Corresponding author. School of Mechanical Engineering and SAINT, Sungkyunkwan University, 2066, Seobu-Ro, Jangan-Gu, Suwon, Gyeong Gi-Do 440-746, Republic of Korea. Tel.: +82 31 299 4843; fax: +82 31 290 5889.

E-mail addresses: [jaehoonkim@skku.edu](mailto:jaehoonkim@skku.edu), [kjh0508@gmail.com](mailto:kjh0508@gmail.com) (J. Kim).

academic and commercial areas [1,2]. LiCoO<sub>2</sub> and graphite, which are currently used for portable electronic devices, are considered not suitable for use in large-scale applications due to the safety concerns and high cost of Co. Lithium phosphates (LiMPO<sub>4</sub>, M = Fe, Mn, Co) [3], lithium orthosilicates (Li<sub>2</sub>MSiO<sub>4</sub>, M = Fe, Mn, Co, Ni) [4], lithium titanium oxides (Li<sub>4</sub>Ti<sub>5</sub>O<sub>12</sub>), and titanium dioxide (TiO<sub>2</sub>) [5] are of particular interest as alternative active materials due to their safety, low cost, environmental friendliness, and high theoretical capacities. However, the major drawback of the alternative materials is their inherently low electronic conductivities and low ionic conductivities; thus, these materials typically suffer from poor rate-capability [3–6].

The reduction of particle size to a nanoscale dimension to enhance lithium ion diffusivity [7,8] and carbon coating to increase electronic conductivity [9,10] are the most widely used strategies to improve the performance of the potential active materials. Nano-sized particles, however, also result in other undesirable effects such as poor energy density and poor electron transport by particle agglomeration in conductive additive matrix. In addition, the increased surface area by reducing particle size can increase side reactions at the electrode-electrolyte interface, which leads to degradation of composite electrode and capacity decay [6]. Incorporation of too much carbon content, thick carbon layer coating, and non-uniform carbon coating on individual particles can also deteriorate energy density and battery performance [6,11–13]. For example, a carbon layer that is too thick can hinder lithium ion diffusion at a high charge/discharge rate [13]. The complete, uniform, and thin carbon layer coverage ensures that the particles receive electrons from all directions and the electrons penetrate easily through the carbon layer, resulting in low polarization and high-rate performance [10,14]. Thus, in view of simple composite electrode processing, high energy density, and high battery performance, finding an effective way to coat an ultrathin and uniform carbon layer on micron-sized active materials, that can result in satisfactory rate performance, needs to be given careful attention. Although many approaches have been proposed to form a uniform carbon layer on individual particles such as *in situ* polymerization [14], double carbon coating [15], and chemical vapor deposition [16], considerable efforts are still underway to develop more reliable, simpler, and less-expensive techniques that can produce the complete coverage of the ultrathin carbon layer on irregular-shaped individual particles and particle agglomerates.

In this paper, we describe the first use of liquid carbon dioxide (*l*-CO<sub>2</sub>) for uniform and ultrathin carbon layer coverage on nano-to-micron-sized LiFePO<sub>4</sub> (LFP) particles. The extremely low surface tension of *l*-CO<sub>2</sub> (0.00195 J m<sup>-2</sup> at 15 °C) makes it an excellent wetting agent and facilitates the penetration of carbon precursors into small pores between particle agglomerates. In addition, the low surface tension of *l*-CO<sub>2</sub>, combined with the ability to decouple the coating from solvent evaporation, can alleviate other non-uniformities caused by high surface tension during solvent drying. The low viscosity of *l*-CO<sub>2</sub> (0.000074 N s m<sup>-2</sup> at 15 °C) can result in thin films and can facilitate carbon precursor diffusion into small pore structures. In addition to the potential to form uniform coating, *l*-CO<sub>2</sub> is non-toxic, non-flammable, and abundant, so that sustainable and clean coating process can be possibly developed. In previous literature, it has been shown that highly uniform and ultrathin organic and polymeric film can be coated on a planar substrate or a highly porous water treatment membrane using high-pressure free-meniscus coating (hFMC) with *l*-CO<sub>2</sub> as the coating solvent [17–20]. Free-meniscus coating is a simple and well-established method to deposit a liquid or a solid film by immersing a substrate in a solution vessel, withdrawing the substrate or draining the solution, and drying the solvent. Herein, we demonstrate that complete coverage of a uniform and ultrathin

carbon layer on LFP particles can be obtained by hFMC with *l*-CO<sub>2</sub> with subsequent calcination at a mild condition.

## 2. Materials and methods

Detailed description on materials, synthesis of LFP and coating procedure is given in the supplementary data. A schematic representing the synthesis of carbon-coated LFP (C-LFP) using *l*-CO<sub>2</sub> hFMC is shown in Fig. 1. Details on the *l*-CO<sub>2</sub> hFMC apparatus are shown in Fig. S1. The LFP particles were placed in a high-pressure coating vessel and sucrose octaacetate (SOA) as a carbon precursor dissolved in *l*-CO<sub>2</sub> was charged into the vessel. Because of its high solubility in *l*-CO<sub>2</sub>, SOA was used as the carbon precursor in this study. It is noted that other carbon precursors that are well-soluble in *l*-CO<sub>2</sub> can be also used as carbon precursors. The *l*-CO<sub>2</sub> solution was drained at the bottom of the vessel, so that SOA was coated on the LFP particles by solution film entrainment. The evaporation of *l*-CO<sub>2</sub> was controlled by adjusting the evaporation driving force ( $\Delta P$ ) to 2 MPa. The SOA-coated LFP (SOA-LFP) was then calcined under a 5 wt.% H<sub>2</sub>/Ar flow condition at 600 °C for 3 h, producing C-LFP-CO<sub>2</sub>.

## 3. Results and discussion

The formation of a highly crystalline LFP phase using a solid-state method can be seen in the X-ray diffraction (XRD) patterns (Fig. S2). All the peaks can be indexed as the olivine LFP phase. Primary LFP particles with sizes of 150–350 nm are highly agglomerated and pores with diameters of 100–250 nm between the particles are observed (Fig. S3). After *l*-CO<sub>2</sub> hFMC, SOA films on LFP particles and SOA nanowires that are connected between the SOA-LFP agglomerates are visible (Fig. 2a). The SOA nanowires are also observed in SOA-LFP prepared at the low SOA concentrations of 9–20 wt.% (Fig. S4). The evaporation of *l*-CO<sub>2</sub> during the solution drainage may cause the nanowire to form by SOA precipitation between the particles. After the calcination, the SOA films are not observed in the SEM image (Fig. 2b), but carbon nanowires connected between the particles are clearly visible (Fig. S5). The phase structure of LFP is maintained under the mild carbon coating condition (Fig. S2) and the carbon formation can be confirmed by Raman spectra (Fig. S6). The uniform and conformal coverage of the carbon layer on LFP with a thickness of 3.3 nm is shown in Fig. 2c and Fig. S7. The carbon map shown in Fig. 2d exhibited a uniform distribution of carbon on the LFP particle. Thus, electrons are expected to access the particles from all directions, which is expected to enhance the electrochemical performance of the active material. When a conventional aqueous solution-based carbon coating method is used, however, the LFP surface is not uniformly covered with a thin carbon layer, as shown in Fig. S8 (C-LFP-H<sub>2</sub>O) and reported previously [21]. In addition, an amorphous carbon region partially covering the LFP surface is observed. The significantly greater uniform coverage of the carbon layer on LFP prepared using *l*-CO<sub>2</sub> hFMC is possibly a result of the facilitated penetration of the coating solution and uniform solution entrainment on individual LFP particles by using the benefits of the low surface tension and low viscosity of *l*-CO<sub>2</sub>.

The galvanostatic charge–discharge curves at 0.1 C rate, along with the cycling performance up to 30 cycles of bare LFP, C-LFP-CO<sub>2</sub>, C-LFP-H<sub>2</sub>O at room temperature, are shown in Fig. 3. The carbon content in the C-LFP is presented in the parenthesis of each sample code. The bare LFP shows a low initial discharge capacity of 90 mAh g<sup>-1</sup> and a large polarization due to poor electronic conductivity. The Li/C (1.9 wt.%)–LFP-CO<sub>2</sub> cell exhibits an extremely flat voltage plateau at ~3.4 V (vs. Li) during the charge–discharge process, which corresponds to the two-phase solid-state reaction

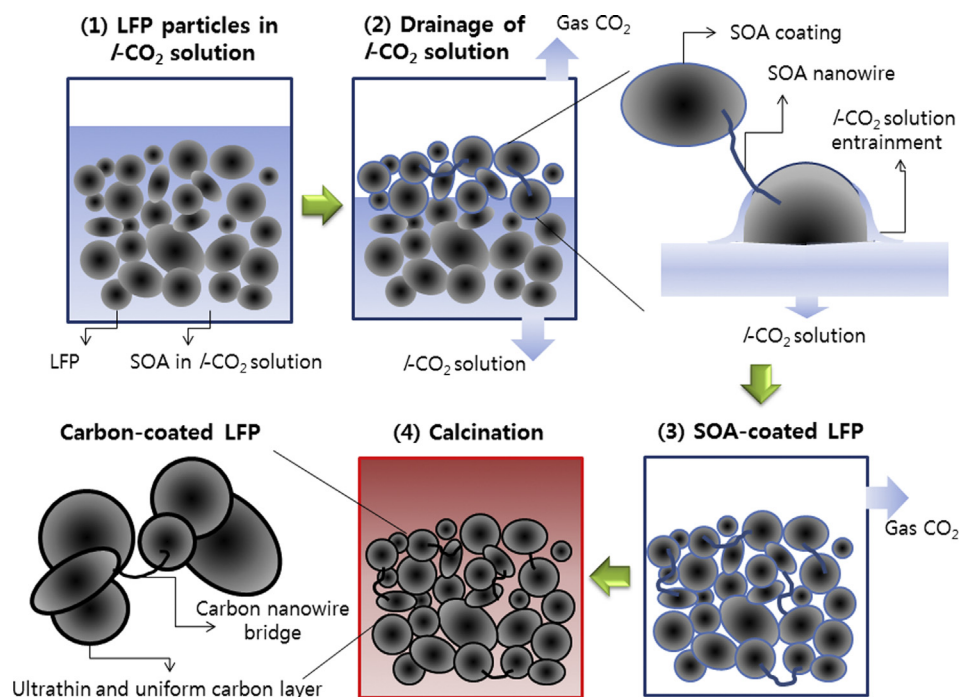


Fig. 1. Schematic of carbon coating procedure by hFMC with  $I\text{-CO}_2$  with subsequent calcination.

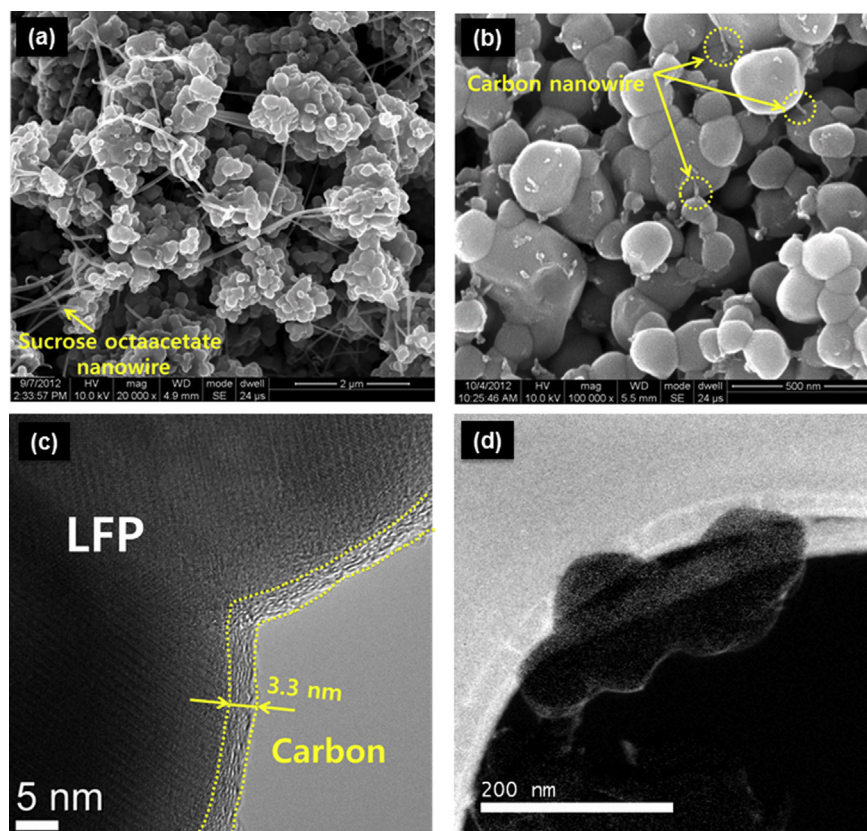


Fig. 2. (a) SEM image of SOA-LFP prepared at 33 wt.% SOA concentration, (b) SEM and (c) HR-TEM images of C-LFP- $\text{CO}_2$ , and (d) element map of carbon in C-LFP- $\text{CO}_2$  by zero-loss TEM measurement. White areas are rich in carbon. The carbon content was 1.9 wt.%.

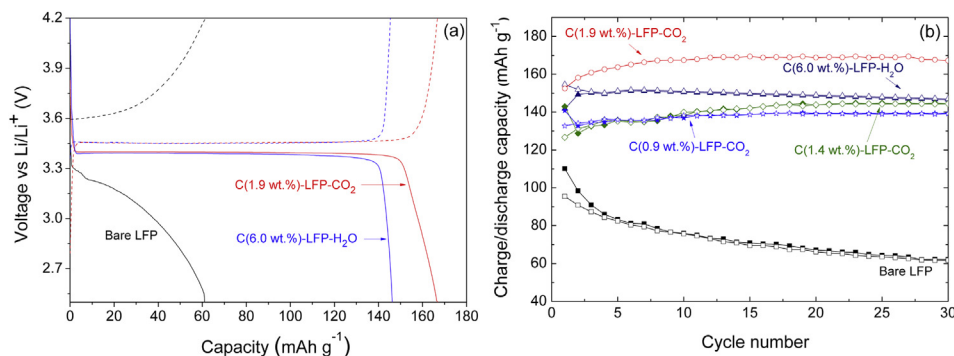


Fig. 3. (a) Charge–discharge profiles of bare LFP and C-LFP at 0.1 C rate after 30 cycles, and (b) cycling performance of bare LFP and C-LFP at 0.1 C rate.

between  $\text{LiFe(II)PO}_4$  and  $\text{Fe(III)PO}_4$ . The discharge capacity of C-LFP- $\text{CO}_2$  gradually increases with cycling at 0.1 C (Fig. 3b), which is probably due to the electrical contact integrity improvement between the LFP, carbon black, and electrode during the charge–discharge process [12]. After 10 cycles, the discharge capacity of C (1.9 wt.%)–LFP- $\text{CO}_2$  increases up to  $169 \text{ mAh g}^{-1}$  at 0.1 C rate, which is very close to the theoretical capacity of LFP ( $170 \text{ mAh g}^{-1}$ ). This result indicates that theoretical capacity of LFP can be reached if electronic conductivity is no longer a problem. In contrast, C (6.0 wt.%)–LFP- $\text{H}_2\text{O}$  exhibits lower discharge capacity of  $146 \text{ mAh g}^{-1}$  at 0.1 C. It is noted that the carbon content, 6.0 wt.%, of C-LFP- $\text{H}_2\text{O}$  was optimized previously to achieve high battery performance [21]. As shown in Fig. 3b, C-LFP- $\text{CO}_2$  with 1.4 wt.% carbon exhibits similar capacity to C-LFP- $\text{H}_2\text{O}$  with 6.0 wt.% carbon. This clearly indicates that the carbon content can be reduced by coating uniform and ultrathin layer on the LFP particles, which possibly increase the volumetric energy density of the composite electrode.

The high-rate performance of C (1.9 wt.%)–LFP- $\text{CO}_2$  and C (6.0 wt.%)–LFP- $\text{H}_2\text{O}$  at various C rates of 0.1–30 C, along with cycling performance up to 150 cycles is presented in Fig. 4. C-LFP- $\text{CO}_2$  exhibits higher discharge capacity at a given C-rate than C-LFP- $\text{H}_2\text{O}$ . The difference in discharge capacities of C-LFP- $\text{CO}_2$  and C-LFP- $\text{H}_2\text{O}$  is more significant at higher C-rates; at 1.0 C, the discharge capacities of C-LFP- $\text{CO}_2$  and C-LFP- $\text{H}_2\text{O}$  are 143 and  $133 \text{ mAh g}^{-1}$ , respectively, while at 30 C rate, those of C-LFP- $\text{CO}_2$  and C-LFP- $\text{H}_2\text{O}$  are 71 and  $17 \text{ mAh g}^{-1}$ , respectively. In addition, when cycling at 1.0 C, a more significant reduction in the polarization loss of C-LFP- $\text{H}_2\text{O}$  is observed when compared to C-LFP- $\text{CO}_2$  (Fig. S9). The much higher discharge capacity at higher C-rates of C-LFP- $\text{CO}_2$  is probably because the uniform and ultrathin carbon layer coated on

individual LFP particles results in faster Li ion transport as well as electron transport in the LFP phase, even though a much lower carbon content is used in C-LFP- $\text{CO}_2$ .

As listed in Table S1, C-LFP- $\text{CO}_2$  with 1.9 wt.% carbon exhibits comparable or better high-rate performance than the other C-LFP with higher carbon content; e.g., double carbon-coated LFP (6.2 wt.%) [11], polyacene-coated LFP (8.5 wt.%) [9], C-LFPs by carbon vapor deposition (2.28 wt.%) [12], by chemical vapor deposition (10.9 wt.%) [16], by a sol–gel method (3.2 wt.%) [13], and by a hydrothermal method (12 wt.%) [22]. The lower rate performance of C (1.9 wt.%)–LFP- $\text{CO}_2$  compared to C-LFP prepared by *in situ* polymerization (6 wt.%) [14], hierarchical mesoporous C-LFP (3.1 wt.%) [15], and multi-wall carbon nanotube-nanorod LFP (8 wt.%) [23] might be due to the use of less carbon content. It might also be because the bare LFP used in this study was larger in size, highly agglomerated, and did not retain nanostructured morphology, so that Li ion diffusion into the LFP structure was intrinsically more hindered. It is noted that the *l*- $\text{CO}_2$  hFMC coating method can be applicable for forming uniform carbon coating on nanostructured particles because of the simple penetration of the solution into nanostructured substrate and uniform coating ability.

In conclusion, a novel carbon coating method to form a complete and ultrathin carbon layer on LFP particles is developed. With a much smaller amount of carbon used, C-LFP prepared by *l*- $\text{CO}_2$  hFMC exhibits much better battery performance than C-LFP prepared by the typical aqueous solution-based method. The carbon coating strategy developed in this study should be applicable to other potential active materials that have low electronic conductivity, including  $\text{Li}_4\text{Ti}_5\text{O}_{12}$ ,  $\text{TiO}_2$ , and  $\text{Li}_2\text{FeSiO}_4$ .

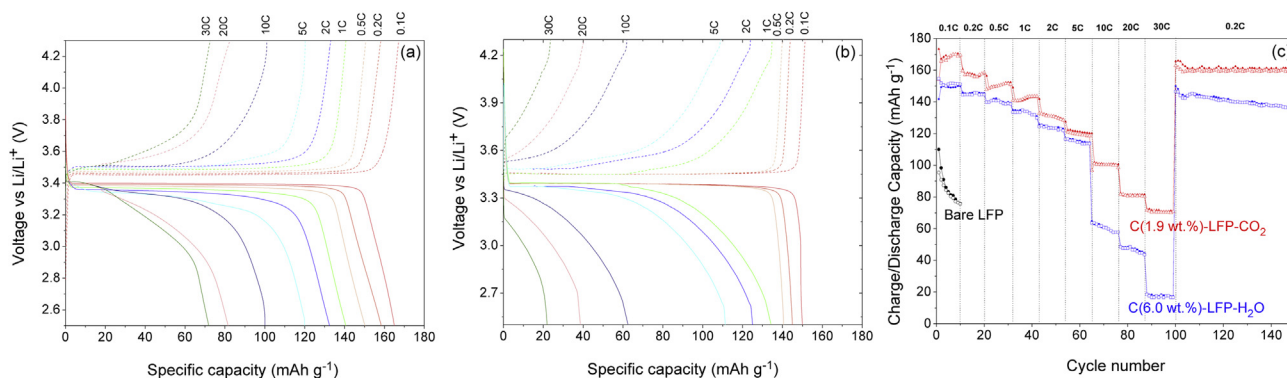


Fig. 4. Charge–discharge profiles of (a) C-LFP (1.9 wt.%)– $\text{CO}_2$  and (b) C-LFP (6.0 wt.%)– $\text{H}_2\text{O}$  at various C-rates of 0.1–30 C, and (c) high-rate performance of C-LFP with variable C-rates.

## Acknowledgments

This research was supported by the National Research Foundation of Korea Grant funded by the Ministry of Science, ICT & Future Planning (2009-0083540 and NRF-2013R1A1A2061020).

## Appendix A. Supplementary data

Supplementary data related to this article can be found in the online version at <http://dx.doi.org/10.1016/j.jpowsour.2014.03.132>.

## References

- [1] V. Etacheri, R. Marom, R. Elazari, G. Salitra, D. Aurbach, *Energy Environ. Sci.* 4 (2011) 3243–3262.
- [2] O.K. Park, Y. Cho, S. Lee, H.-C. Yoo, H.-K. Song, J. Cho, *Energy Environ. Sci.* 4 (2011) 1621–1633.
- [3] P.S. Herle, B. Ellis, N. Coombs, L.F. Nazar, *Nat. Mater.* 3 (2004) 147–152.
- [4] M.S. Islam, R. Dominko, C. Masquelier, C. Sirisopanaporn, A.R. Armstrong, P.G. Bruce, *J. Mater. Chem.* 21 (2011) 9811–9818.
- [5] Z. Yang, D. Choi, S. Kerisit, K.M. Rosso, D. Wang, J. Zhang, G. Graff, J. Liu, *J. Power Sources* 192 (2009) 588–598.
- [6] J. Wang, X. Sun, *Energy Environ. Sci.* 5 (2012) 5163–5185.
- [7] C. Delacourt, P. Poizot, S. Levasseur, C. Masquelier, *Electrochem. Solid-State Lett.* 9 (2006) A352–A355.
- [8] A. Nugroho, W. Chang, S.J. Kim, K.Y. Chung, J. Kim, *RSC Adv.* 2 (2012) 10805–10808.
- [9] H.-M. Xie, R.-S. Wang, J.-R. Ying, L.-Y. Zhang, A.F. Jalbout, H.-Y. Yu, G.-L. Yang, X.-M. Pan, Z.-M. Su, *Adv. Mater.* 18 (2006) 2609–2613.
- [10] H. Li, H. Zhou, *Chem. Commun.* 48 (2012) 1201–1217.
- [11] Z. Chen, J.R. Dahn, *J. Electrochem. Soc.* 149 (2002) A1184–A1189.
- [12] Y.-D. Cho, G.T.-K. Fey, H.-M. Kao, *J. Power Sources* 189 (2009) 256–262.
- [13] R. Dominko, M. Bele, M. Gaberscek, M. Remskar, D. Hanzel, S. Pejovnik, J. Jamnik, *J. Electrochem. Soc.* 152 (2005) A607–A610.
- [14] Y. Wang, Y. Wang, E. Hosono, K. Wang, H. Zhou, *Angew. Chem. Int. Ed.* 47 (2008) 7461–7465.
- [15] S.W. Oh, S.-T. Myung, S.-M. Oh, K.H. Oh, K. Amine, B. Scrosati, Y.-K. Sun, *Adv. Mater.* 22 (2010) 4842–4845.
- [16] B. Zhao, Y. Jiang, H. Zhang, H. Tao, M. Zhong, Z. Jiao, *J. Power Sources* 189 (2009) 462–466.
- [17] J. Kim, B.J. Novick, J.M. De Simone, R.G. Carbonell, *Langmuir* 22 (2006) 642–657.
- [18] J. Kim, R.G. Carbonell, *J. Supercrit. Fluids* 42 (2007) 129–141.
- [19] J. Kim, K. Efimenko, J. Genzer, R.G. Carbonell, *Macromolecules* 40 (2007) 588–597.
- [20] J.-H. Kim, J.P. Rolland, R.G. Carbonell, J.M. De Simone, *Chem. Mater.* 22 (2010) 2411–2413.
- [21] S.-A. Hong, S.J. Kim, J. Kim, B.G. Lee, K.Y. Chung, Y.-W. Lee, *Chem. Eng. J.* 198–199 (2012) 318–326.
- [22] S. Yoon, C. Liao, X.-G. Sun, C.A. Bridges, R.R. Unocic, J. Nanda, S. Dai, M.P. Paranthaman, *J. Mater. Chem.* 22 (2012) 4611–4614.
- [23] T. Muraliganth, A.V. Murugan, A. Manthiram, *J. Mater. Chem.* 18 (2008) 5661–5668.